JACS
JOURNAL OF THE AMERICAN CHEMICAL SOCIETY
Communication
pubs.acs.org/JACS

Chemical Synthetic Strategy for Single-Layer Transition-Metal Chalcogenides

Dongwon Yoo,† Minkyoung Kim,† Sohee Jeong, Jeonghee Han, and Jinwoo Cheon*

Department of Chemistry, Yonsei University, Seoul 120-749, Korea

Supporting Information

ABSTRACT: A solution-phase synthetic protocol to form two-dimensional (2D) single-layer transition-metal chalcogenides (TMCs) has long been sought; however, such efforts have been plagued with the spontaneous formation of multilayer sheets. In this study, we discovered a solution-phase synthetic protocol, called "diluted chalcogen continuous influx (DCCI)", where controlling the chalcogen source influx (e.g., H_2S) during its reaction with the transition-metal halide precursor is the critical parameter for the formation of single-layer sheets as examined for the cases of group IV TMCs. The continuous influx of dilute H_2S throughout the entire growth period is necessary for large sheet formation through the exclusive *a*- and *b*-axial growth processes. By contrast, the burst influx of highly concentrated H_2S in the early stages of the growth process forms multilayer TMC nanodiscs. Our DCCI protocol is a new synthetic concept for single-layer TMCs and, in principle, can be operative for wide range of TMC nanosheets.

Two-dimensional (2D) single-layer transition-metal chalcogenides (TMCs) have recently received tremendous attention after the observation of unique material properties which are different from multilayer or bulk phase TMCs.[1] Their physicochemical properties, such as conductivity, absorption, and quantum efficiency, are greatly affected by the number of layers[2] and, in particular, electronic band structure changes from indirect for bulk TMCs to direct for single-layer TMCs.[3] Single-layer TMCs are considered as next generation 2D materials especially for applications such as optoelectronics, photocatalysis, and solar energy harvesting.[4] Currently, gas-phase chemical vapor deposition (CVD) and mechanical exfoliation techniques are the two most established approaches for the preparation of single-layer TMC nanosheets; however, neither are perfect yet and tremendous efforts are currently being made to improve issues such as controllability over size and thickness, reproducibility, and mass production.[5]

Although solution-phase synthetic methods are advantageous for their simple synthetic procedures and relatively easy scale-up as proven in earlier reports,[6] their synthetic implementation for single-layer 2D TMCs has been challenging. Recent reports suggest new possibilities for obtaining single-layer TMC nanosheets;[7,8] however, these methods also reveal their limitations. Notably, single-layer 2D TMCs being present during the early growth period are readily forming multilayer 2D nanosheets. Continuous lateral growth of TMCs while keeping them in a single-layer has been one of the challenges to overcome.

Here, we successfully developed a solution-phase synthetic protocol, DCCI, which provides the formation of single-layer sheet with a large lateral dimension for group IV TMCs. One key observation is that the slow and continuous influx of the chalcogen source (e.g., H_2S) into the reaction medium makes selective growth in the lateral (*a*-, *b*-axis) direction (Scheme 1).

Scheme 1. Single- vs Multilayer Transition-Metal Sulfide Nanosheets[a]

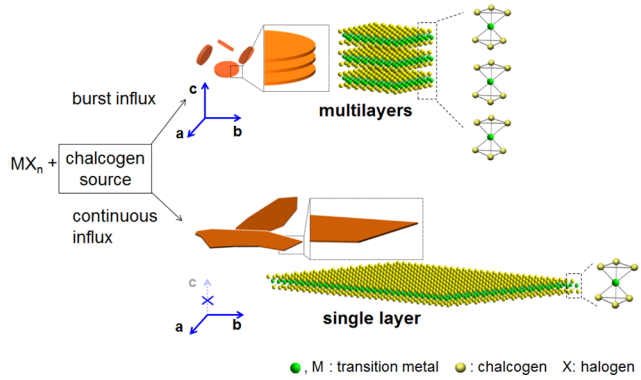

[a]Single-layer TMCs with 1T structure consisting of chalcogen−metal−chalcogen triatomic layers. Finding a kinetic growth regime, where lateral growth in high-energy surface (*a*-, *b*-axis) continues, while the low-energy surface (*c*-axis) growth is prohibited, is key to generate single-layer sheets. Upon its reaction with the metal halide precursors (MX_n; X= halogen), a dilute and continuous supply of the chalcogen source throughout the entire reaction yields single-layer nanosheets, whereas a rapid and highly concentrated supply of the chalcogen source during the beginning of the reaction generates multilayer structures (see *vide infra*).

As a representative case of this study, we choose ZrS_2 among the various TMCs to examine the possibility of single-layer sheet formation. Each layer of ZrS_2 comprises a S−Zr−S triatomic octahedral structure corresponding to 1T-ZrS_2 (Scheme 1). We use 1-dodecanethiol (DDT, 5.0 mmol) as sulfur precursor for the *in situ* formation of H_2S, a reactive chalcogen source, which reacts with $ZrCl_4$ (0.3 mmol) in oleylamine at 245 °C (Figure 1a). The reaction is maintained for 10 h and centrifuged to isolate the ZrS_2 nanosheets. TEM analysis shows that the products are single-layer nanosheets

Received: August 4, 2014
Published: October 14, 2014

   dx.doi.org/10.1021/ja5079943 | J. Am. Chem. Soc. 2014, 136, 14670−14673

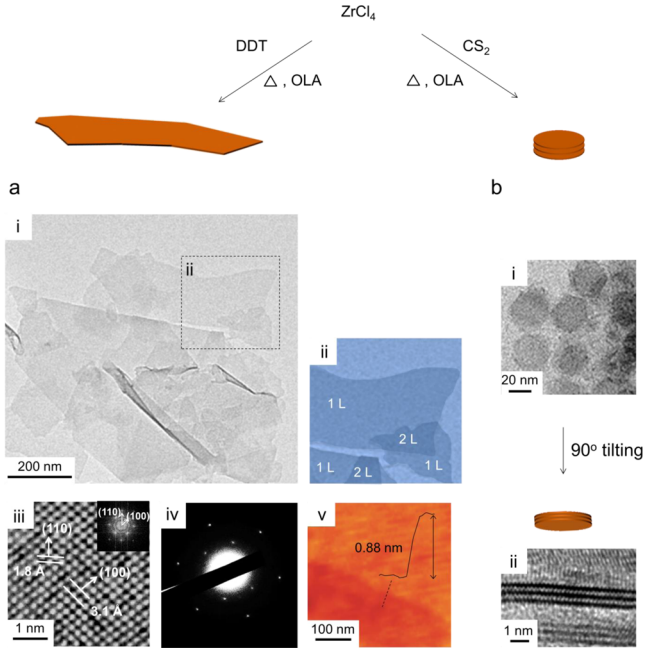

Figure 1. Formation of single-layer ZrS_2 nanosheets and multilayer nanodiscs with the use of different chalcogen precursors. (a) Characterization of the single-layer ZrS_2 nanosheets: (i) TEM image of the single-layer ZrS_2 nanosheets; (ii) pseudocolor image of a small area (L: layer); (iii) HRTEM image and FFT pattern (inset); (iv) SAED pattern; and (v) AFM image. (b) Characterization of the multilayer ZrS_2 nanodiscs: (i) TEM image of ZrS_2 nanodiscs and (ii) high-magnification TEM image of the ZrS_2 nanodiscs side view. DDT: 1-dodecanethiol, OLA: oleylamine.

with ~200−500 nm in lateral size (Figure 1a(i)). A pseudocolor image of a selected area is provided to clearly visualize the some overlay between the single-layer ZrS_2 nanosheets (Figure 1a(ii)). A top-view high-resolution transmission electron microscopy (HRTEM) image of the ZrS_2 nanosheet reveals the periodic atomic arrangement by showing lattice fringes with interplanar spacings of 3.1 and 1.8 Å corresponding to the (100) and (110) planes, respectively, in the hexagonal 1T-ZrS_2 (Figure 1a(iii)). The fast Fourier transform (FFT) image of the ZrS_2 nanosheet shows hexagonal patterns corresponding to the (100) and (110) reflections from the top view (Figure 1a(iii) inset). The selected area electron diffraction (SAED) pattern for the ZrS_2 nanosheets confirms their high crystallinity (Figure 1a(iv)). The atomic force microscopy (AFM) image shown in Figure 1a(v) indicates a nanosheet with a height of ~0.88 nm, which is consistent with the formation of a single layer. Additional XRD analysis shows the absence of (001) peak, indicating the formation of single-layer ZrS_2 (Figure S2a).

By contrast, when we performed an identical reaction except using CS_2 as an alternative sulfur precursor, multilayer ZrS_2 nanodiscs resulted; such an outcome is consistent with previous studies (Figure 1b).[9] A top-view TEM image of the synthesized ZrS_2 nanodiscs shows a uniform, free-standing disc-like morphology with ~20 nm in lateral size (Figure 1b(i)), and a side-view image indicates that the number of layers is three (Figure 1b(ii)).

For detailed information on the *in situ* generation of H_2S, we investigated the H_2S generation kinetics for DDT[10] and CS_2[11] under identical crystal growth conditions via the standard methylene blue method.[12] H_2S generated from each precursor at 245 °C in the presence of oleylamine is collected into the reaction mixture of *N*,*N*-dimethyl-1,4-phenylenediamine and $FeCl_3$ in a 6 M aqueous HCl solution to convert the H_2S into methylene blue (Figure 2a). The generation of methylene blue

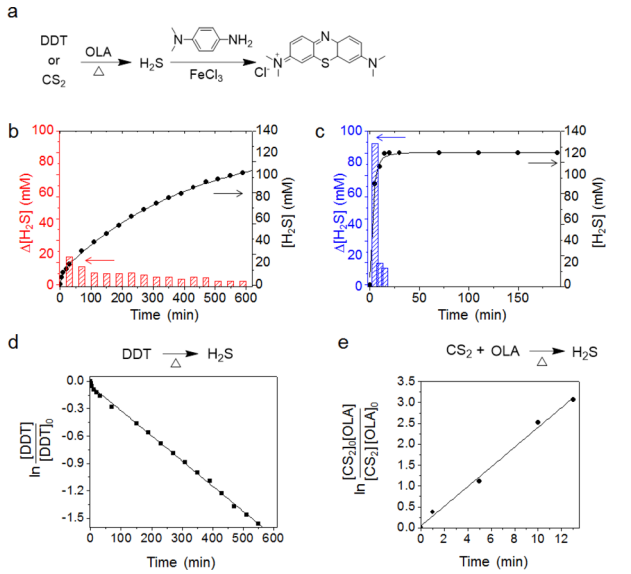

Figure 2. *In situ* H_2S generation kinetics from DDT and CS_2. (a) Methylene blue assay is used for the quantification of H_2S. (b) Time-dependent cumulative H_2S generation profile from DDT (black dots) and the H_2S concentration for a given time interval (40 min, red bars), which indicates that H_2S is continuously generated over a long reaction period (10 h). (c) Time-dependent cumulative H_2S profile from CS_2 (black dots) and H_2S concentration for a given time interval (5 min, blue bars), where the H_2S generation is initially very high but stops after 20 min. (d) First-order reaction kinetics of H_2S generation from DDT. (e) Second-order reaction kinetics of H_2S generation using CS_2 and OLA.

is then monitored by using a UV−vis absorption spectrometer. The total amount H_2S produced by DDT gradually increases (black dots, Figure 2b) up to ~100 mM for the entire reaction period (10 h). For each measured time segment (40 min), the H_2S influx holds steady between 12 and 3 mM from 1 to 10 h period after a slightly higher H_2S influx (~19 mM) during the first 40 min (red bars, Figure 2b).

In case of CS_2, the amount of generated H_2S increases drastically at the initial temporal point and reaches a maximum of ~120 mM in 20 min with a plateau afterward (black dots, Figure 2c). After the burst influx of H_2S during the first 15 min (blue bars, Figure 2c), the H_2S influx drops down to zero from 20 to 180 min time period. The amount of generated H_2S is 92 mM in the first 5 min. We observed that H_2S generation from the thermolysis of DDT is a unimolecular reaction following first-order kinetics with a reaction rate constant of 2.8×10^{-3} s^{-1} (Figure 2d). By contrast, the kinetic plot presented in Figure 2e shows that H_2S generation from CS_2 follows second-order kinetics, confirming that H_2S generation is a bimolecular reaction between CS_2 and oleylamine with a reaction rate constant of 2.4×10^{-1} L $mol^{-1}s^{-1}$. The *in situ* H_2S generation rate from CS_2 is ~86 times faster than that from DDT.

The growth kinetics of colloidal nanostructures is governed by a number of parameters, and one of them is the concentration of monomers.[13] As shown here, the distinct kinetic differences between DDT and CS_2 for H_2S influx into the reaction medium can be the determining factor for different

dx.doi.org/10.1021/ja5079943 | J. Am. Chem. Soc. 2014, 136, 14670−14673

crystal growth patterns. Because the surface energies of the *a*-, *b*-axis edge facets, such as (100) and (110), are approximately 4−6 times higher than that of the *c*-axis planar facet (001),[8b,9] exclusive growth at the edges can be possible, but only when the growth proceeds under specific conditions that can keep their facet energy differences.[14] This study shows that the dilute and continuous influx of H_2S from DDT satisfies such a kinetic growth window for preferential 2D lateral growth. By contrast, the burst H_2S influx from CS_2 generates overly concentrated monomers and disrupts the facet selectivity so that simultaneous growth in both the lateral and vertical directions can take place.[15] Similar growth pattern has been observed for metallic prisms with high monomer concentrations.[16] When we examined another H_2S precursor, thioacetamide, which has similar H_2S generation kinetics with CS_2, multilayer ZrS_2 nanodics are consistently observed (Figure S1).

For the validation of such H_2S influx effects on the growth patterns, H_2S gas is directly introduced into a solution of $ZrCl_4$ and oleylamine (Figure 3a). Rapidly injecting a fixed amount of

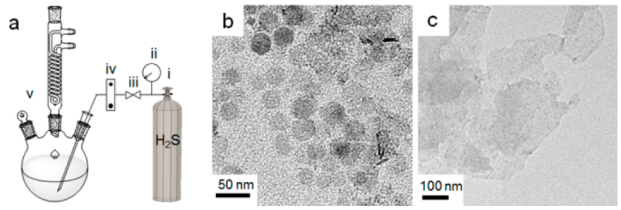

Figure 3. Direct H_2S gas flow experiment. (a) Diagram of the experimental setup consisting of (i) H_2S gas tank; (ii) pressure gauge; (iii) shutoff valve; (iv) flowmeter; and (v) reaction vessel. (b,c) TEM images of the ZrS_2 nanodiscs (b) and nanosheets (c) produced by using rapid and slow H_2S supply, respectively.

H_2S gas in a short time (20 min) following an identical H_2S generation profile of CS_2 provides multilayer ZrS_2 nanodiscs of ~25 nm in diameter (Figure 3b). By contrast, the low and prolonged influx of H_2S gas for 600 min, mimicking the dodecanethiol-mediated reaction, affords much larger ZrS_2 (few hundred nanometers) with a sheet morphology (Figure 3c). Our control study indicates that the lateral size and thickness of the nanosheets are clearly dependent on the H_2S influx kinetics. As a note, the use of gas-phase H_2S does not provide high-quality nanosheets relative to the *in situ* solution-generated cases, possibly due to inhomogeneous mixing and reaction between the gas- and solution-phases during the nucleation and growth processes;[17] however, such direct introduction of chalcogen source also has the potential to generate high quality single-layer TMCs upon further optimization processes.

Our DCCI method is extended for its suitability with other group IV TMC nanosheet, TiS_2 and HfS_2. First, the same synthetic procedures are performed with the introduction of DDT (5.0 mmol) to a mixture of $TiCl_4$ (0.26 mmol) and oleylamine (18.7 mmol) at 230 °C (Figure 4a). The resulting products are single-layer TiS_2 nanosheets ranging between ~300 nm and ~1 μm in lateral size (Figure 4b(i)). The pseudocolor image shows single-layer TiS_2 nanosheets (Figure 4b(ii)). A top-view HRTEM image of the TiS_2 nanosheet indicates the periodic atom arrangements of the lattice fringes with interplanar spacings of 2.9 and 1.7 Å for the (100) and (110) hexagonal 1T-TiS_2 planes, respectively (Figure 4b(iii)). The FFT image of the TiS_2 nanosheet shows a hexagonal pattern corresponding to the (100) and (110) reflections from

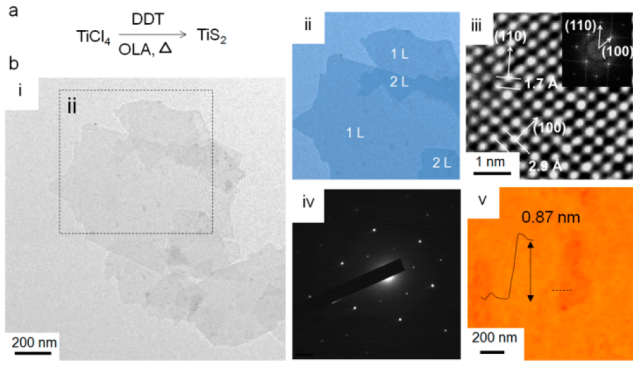

Figure 4. Single-layer TiS_2 nanosheets through DCCI method. (a) Single-layer TiS_2 nanosheets formed by using DDT. (b) (i) Low-magnification TEM image; (ii) pseudocolor image for a selected area; (iii) HRTEM image and FFT pattern (inset); (iv) SAED pattern; and (v) AFM image of a single-layer TiS_2 nanosheet.

the top view (Figure 4b(iii) inset). Figure 4b(iv) is the SAED pattern for the TiS_2 nanosheets confirming the high crystallinity. The AFM image in Figure 4b(v) shows a single-layer 2D sheet with a height of 0.87 nm that is close to the 0.9 nm reported in the literature.[5a,18] XRD analysis confirms single-layer TiS_2 formation (Figure S2b). This DCCI protocol is also effective for single-layer HfS_2 nanosheet formation (Figure 5).

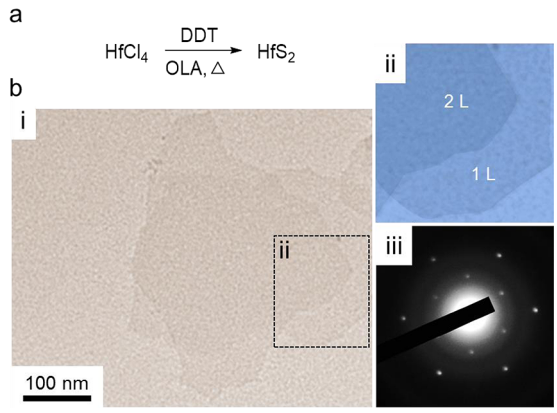

Figure 5. Synthesis of single-layer HfS_2 nanosheets. (a) Chemical reaction for HfS_2. (b) (i) TEM image; (ii) pseudocolor image for a selected area; and (iii) SAED pattern.

Here, we have developed a solution-based synthetic protocol, DCCI, for the formation of single-layer nanosheets of group IV metal sulfides. The control of key synthetic parameters, which renders the continuous growth of lateral facets, is critical, and the dilute and continuous influx of H_2S plays such a role. Our study provides a new synthetic principle that could be potentially useful for the single-layer sheet formation of other 2D layered materials; however, the specific reaction conditions and parameters should be designed prior for each case.

■ ASSOCIATED CONTENT

Ⓢ Supporting Information

Detailed synthetic methods and characterizations. This material is available free of charge via the Internet at http://pubs.acs.org.

■ AUTHOR INFORMATION

Corresponding Author

jcheon@yonsei.ac.kr

dx.doi.org/10.1021/ja5079943 | *J. Am. Chem. Soc.* 2014, 136, 14670−14673

Author Contributions

[†]These authors contributed equally.

Notes

The authors declare no competing financial interest.

■ ACKNOWLEDGMENTS

This work was financially supported by the National Creative Research Initiatives Program (2010-0018286).

■ REFERENCES

(1) (a) Li, H.; Wu, J.; Yin, Z.; Zhang, H. *Acc. Chem. Res.* **2014**, *47*, 1067. (b) Huang, X.; Zeng, Z.; Zhang, H. *Chem. Soc. Rev.* **2013**, *42*, 1934. (c) Chhowalla, M.; Shin, H. S.; Eda, G.; Li, L.-J.; Loh, K. P.; Zhang, H. *Nat. Chem.* **2013**, *5*, 263. (d) Wang, Q. H.; Kalantar-Zadeh, K.; Kis, A.; Coleman, J. N.; Strano, M. S. *Nat. Nanotechnol.* **2012**, *7*, 699. (e) Mattheis, L. F. *Phys. Rev. B* **1973**, *8*, 3719. (f) Wilson, A.; Yoffe, A. D. *Adv. Phys.* **1969**, *18*, 193.

(2) (a) Voiry, D.; Yamaguchi, H.; Li, J.; Silva, R.; Alves, D. C. B.; Fujita, T.; Chen, M.; Asefa, T.; Shenoy, V. B.; Eda, G.; Chhowalla, M. *Nat. Mater.* **2013**, *12*, 850. (b) Lukowski, M. A.; Daniel, A. S.; Meng, F.; Forticaux, A.; Li, L.; Jin, S. *J. Am. Chem. Soc.* **2013**, *135*, 10274. (c) Zhu, C.; Zeng, Z.; Li, H.; Li, F.; Fan, C.; Zhang, H. *J. Am. Chem. Soc.* **2013**, *135*, 5998. (d) Zhang, W.; Huang, J.-K.; Chen, C.-H.; Chang, Y.-H.; Cheng, Y.-J.; Li, L.-J. *Adv. Mater.* **2013**, *25*, 3456. (e) Zhao, W.; Ghorannevis, Z.; Chu, L.; Toh, M.; Kloc, C.; Tan, P.-H.; Eda, G. *ACS Nano* **2013**, *7*, 791.

(3) (a) Kuc, A.; Zibouche, N.; Heine, T. *Phys. Rev. B* **2011**, *83*, 245213. (b) Mak, K. F.; Lee, C.; Hone, J.; Shan, J.; Heinz, T. F. *Phys. Rev. Lett.* **2010**, *105*, 136805. (c) Gordon, R. A.; Yang, D.; Crozier, E. D.; Jiang, D. T.; Frindt, R. F. *Phys. Rev. B* **2002**, *65*, 125407.

(4) (a) Zhou, W.; Yin, Z.; Du, Y.; Huang, X.; Zeng, Z.; Fan, Z.; Liu, H.; Wang, J.; Zhang, H. *Small* **2013**, *9*, 140. (b) Yin, Z.; Li, H.; Li, H.; Jiang, L.; Shi, Y.; Sun, Y.; Lu, G.; Zhang, Q.; Chen, X.; Zhang, H. *ACS Nano* **2012**, *6*, 74. (c) Mak, K. F.; He, K.; Shan, J.; Heinz, T. F. *Nat. Nanotechnol.* **2012**, *7*, 494. (d) Zeng, H.; Dai, J.; Yao, W.; Xiao, D.; Cui, X. *Nat. Nanotechnol.* **2012**, *7*, 490. (e) Radisavljevic, B.; Radenovic, A.; Brivio, J.; Giacometti, V.; Kis, A. *Nat. Nanotechnol.* **2011**, *6*, 147. (f) Chianelli, R. R.; Siadati, M. H.; De la Rosa, M. P.; Berhault, G.; Wilcoxon, J. P.; Bearden, R., Jr.; Abrams, B. L. *Catal. Rev.* **2006**, *48*, 1.

(5) (a) Zheng, J.; Zhang, H.; Dong, S.; Liu, Y.; Nai, C. T.; Shin, H. S.; Jeong, H. Y.; Liu, B.; Loh, K. P. *Nat. Commun.* **2014**, *5*, 2995. (b) Zhang, Y.; Zhang, Y.; Ji, Q.; Ju, J.; Yuan, H.; Shi, J.; Gao, T.; Ma, D.; Liu, M.; Chen, Y.; Song, X.; Hwang, H. Y.; Cui, Y.; Liu, Z. *ACS Nano* **2013**, *7*, 8963. (c) Liu, K.-K; Zhang, W.; Lee, Y.-H.; Lin, Y. C.; Chang, M.-T.; Su, C.-Y.; Chang, C.-S.; Li, H.; Shi, Y.; Zhang, H.; Lai, C.-S.; Li, L.-J. *Nano Lett.* **2012**, *12*, 1538. (d) Lee, Y.-H.; Zhang, X.-Q.; Zhang, W.; Chang, M.-T.; Lin, C.-T.; Chang, K.-D.; Yu, Y.-C.; Wang, J. T.-W.; Chang, C.-S.; Li, L.-J.; Lin, T.-W. *Adv. Mater.* **2012**, *24*, 2320. (e) Coleman, J. N.; Lotya, M.; O'Neill, A.; Bergin, S. D.; King, P. J.; Khan, U.; Young, K.; Gaucher, A.; De, S.; Smith, R. J.; Shvets, I. V.; Arora, S. K.; Stanton, G.; Kim, H.-Y.; Lee, K.; Kim, G. T.; Duesberg, G. S.; Hallam, T.; Boland, J. J.; Wang, J. J.; Donegan, J. F.; Grunlan, J. C.; Moriarty, G.; Shmeliov, A.; Nicholls, R. J.; Perkins, J. M.; Grieveson, E. M.; Theuwissen, K.; McComb, D. W.; Nellist, P. D.; Nicolosi, V. *Science* **2011**, *331*, 568. (f) Zeng, Z.; Yin, Z.; Huang, X.; Li, H.; He, Q.; Lu, G.; Boey, F.; Zhang, H. *Angew. Chem., Int. Ed.* **2011**, *50*, 11093.

(6) (a) Han, J. H.; Lee, S.; Cheon, J. *Chem. Soc. Rev.* **2013**, *42*, 2581. (b) Zhai, T.; Li, L.; Ma, Y.; Liao, M.; Wang, X.; Fang, X.; Yao, J.; Bando, Y.; Golberg, D. *Chem. Soc. Rev.* **2011**, *40*, 2986. (c) Cozzoli, P. D.; Pellegrino, T.; Manna, L. *Chem. Soc. Rev.* **2006**, *35*, 1195. (d) Yin, Y.; Alivisatos, A. P. *Nature* **2005**, *437*, 664. (e) Park, J.; An, K.; Hwang, Y.; Park, J.-G.; Noh, H.-J.; Kim, J.-Y.; Park, J.-H.; Hwang, N.-M.; Hyeon, T. *Nat. Mater.* **2004**, *3*, 891. (f) Li, J. J.; Wang, Y. A.; Guo, W.; Keay, J. C.; Mishima, T. D.; Johnson, M. B.; Peng, X. *J. Am. Chem. Soc.* **2003**, *125*, 12567. (g) Stoeva, S.; Klabunde, K. J.; Sorensen, C. M.; Dragieva, I. *J. Am. Chem. Soc.* **2002**, *124*, 2305. (h) Jana, N. R.; Peng, X. *J. Am. Chem. Soc.* **2003**, *125*, 14280.

(7) (a) Seo, J.-w.; Jun, Y.-w.; Park, S.-w.; Nah, H.; Moon, T.; Park, B.; Kim, J.-G.; Kim, Y. J.; Cheon, J. *Angew. Chem., Int. Ed.* **2007**, *46*, 8828. (b) Park, K. H.; Choi, J.; Kim, H. J.; Oh, D.-H.; Ahn, J. R.; Son, S. U. *Small* **2008**, *4*, 945. (c) Altavilla, C.; Sarno, M.; Ciambelli, P. *Chem. Mater.* **2011**, *23*, 3879.

(8) (a) Sekar, P.; Greyson, E. C.; Barton, J. E.; Odom, T. W. *J. Am. Chem. Soc.* **2005**, *127*, 2054. (b) Jeong, S.; Yoo, D.; Jang, J.-t.; Kim, M.; Cheon, J. *J. Am. Chem. Soc.* **2012**, *134*, 18233. (c) Antunez, P. D.; Webber, D. H.; Brutchey, R. L. *Chem. Mater.* **2013**, *25*, 2385.

(9) Jang, J.-t.; Jeong, S.; Seo, J.-w.; Kim, M.-C.; Sim, E.; Oh, Y.; Nam, S.; Park, B.; Cheon, J. *J. Am. Chem. Soc.* **2011**, *133*, 7636.

(10) Baldridge, K. K.; Gordon, M. S.; Johnson, D. E. *J. Phys. Chem.* **1987**, *91*, 4145.

(11) Ballabeni, M.; Ballini, R.; Bigi, F.; Maggi, R.; Parrini, M.; Predieri, G.; Sartori, G. *J. Org. Chem.* **1999**, *64*, 1029.

(12) (a) Devarie-Baez, N. O.; Bagdon, P. E.; Peng, B.; Zhao, Y.; Park, C.-M.; Xian, M. *Org. Lett.* **2013**, *15*, 2786. (b) Chen, S.; Chen, Z.-j.; Ren, W.; Ai, H.-w. *J. Am. Chem. Soc.* **2012**, *134*, 9589. (c) Lawrence, N. S.; Davis, J.; Compton, R. G. *Talanta* **2000**, *52*, 771. (d) Moest, R. R. *Anal. Chem.* **1975**, *47*, 1204. (e) Fogo, J. K.; Popowsky, M. *Anal. Chem.* **1949**, *21*, 732.

(13) (a) Wang, X.; Peng, Q.; Li, Y. *Acc. Chem. Res.* **2007**, *40*, 635. (b) Jun, Y.-w.; Choi, J.-s.; Cheon, J. *Angew. Chem., Int. Ed.* **2006**, *45*, 3414. (c) Kumar, S.; Nann, T. *Small* **2006**, *2*, 316.

(14) (a) Peng, X. *Adv. Mater.* **2003**, *15*, 459. (b) Peng, Z. A.; Peng, X. *J. Am. Chem. Soc.* **2001**, *123*, 1389. (c) Manna, L.; Scher, E. C.; Alivisatos, P. A. *J. Am. Chem. Soc.* **2000**, *122*, 12700.

(15) Kudera, S.; Carbone, L.; Manna, L.; Parak, W. Growth mechanism, shape and composition control of semiconductor nanocrystals. In *Semiconductor Nanocrystal Quantum Dots*; Rogach, A. L., Ed.; Springer-Verlag: Wien, Austria, 2008; pp 1−34.

(16) Xue, C.; Métraux, G. S.; Millstone, J. E.; Mirkin, C. A. *J. Am. Chem. Soc.* **2008**, *130*, 8337.

(17) Gardeniers, J. G. E. Multiphase Reactions. In *Microchemical Engineering in Practice*; Dietrich, T. R., Ed.; John Wiley & Sons: Hoboken, NJ, 2011; pp 449−474.

(18) Zeng, Z.; Tan, C.; Huang, X.; Bao, S.; Zhang, H. *Energy Environ. Sci.* **2014**, *7*, 797.